for more complex sites: The side-chain identity and conformation combinatorics dealt with by hashing in RosettaMatch become intractable for sites consisting of five or more long polar side chains, which for accurate representation may require as many as 1000 rotamer conformations each. At the other extreme, bound water molecules offer considerable versatility, because they can readily reorient to switch between acting as hydrogen-bond acceptors and donors and involve neither delicate free-energy tradeoffs nor intricate interaction networks.

It is tempting to speculate that our computationally designed enzymes resemble primordial enzymes more than they resemble highly refined modern-day enzymes. The ability to design simultaneously only three to four catalytic residues parallels the infinitesimal probability that, early in evolution, more than three to four residues would have happened to be positioned appropriately for catalysis; some of the functions played by exquisitely positioned side chains in modern enzymes may have been played by water molecules earlier in evolutionary history.

Although our results demonstrate that novel enzyme activities can be designed from scratch and indicate the catalytic strategies that are most accessible to nascent enzymes, there is still a significant gap between the activities of our designed catalysts and those of naturally occurring enzymes. Narrowing this gap presents an exciting prospect for future work: What additional features have to be incorporated into the design process to achieve catalytic activities approaching those of naturally occurring enzymes? The close agreement between the two crystal structures and the design models gives credence to our strategy of testing hypotheses about catalytic mechanisms by generating and testing the corresponding designs; indeed, almost any idea about catalysis can be readily tested by incorporation into the computational design procedure. Determining what is missing from the current generation of designs and how it can be incorporated into a next generation of more active designed catalysts will be an exciting challenge that should unite the fields of enzymology and computational protein design in the years to come.

References and Notes

1. D. K. Ro *et al.*, *Nature* **440**, 940 (2006).
2. O. Kirk, T. V. Borchert, C. C. Fuglsang, *Curr. Opin. Biotechnol.* **13**, 345 (2002).
3. D. B. Janssen, I. J. Dinkla, G. J. Poelarends, P. Terpstra, *Environ. Microbiol.* **7**, 1868 (2005).
4. D. Hilvert, *Annu. Rev. Biochem.* **69**, 751 (2000).
5. B. Seelig, J. W. Szostak, *Nature* **448**, 828 (2007).
6. F. H. Arnold, A. A. Volkov, *Curr. Opin. Chem. Biol.* **3**, 54 (1999).
7. O. Khersonsky, C. Roodveldt, D. S. Tawfik, *Curr. Opin. Chem. Biol.* **10**, 498 (2006).
8. B. Kuhlman *et al.*, *Science* **302**, 1364 (2003).
9. L. L. Looger, M. A. Dwyer, J. J. Smith, H. W. Hellinga, *Nature* **423**, 185 (2003).
10. D. N. Bolon, S. L. Mayo, *Proc. Natl. Acad. Sci. U.S.A.* **98**, 14274 (2001).
11. J. Kaplan, W. F. DeGrado, *Proc. Natl. Acad. Sci. U.S.A.* **101**, 11566 (2004).
12. F. Tanaka, R. Fuller, H. Shim, R. A. Lerner, C. F. Barbas III, *J. Mol. Biol.* **335**, 1007 (2004).
13. A. Heine *et al.*, *Science* **294**, 369 (2001).
14. S. W. Fullerton *et al.*, *Bioorg. Med. Chem.* **14**, 3002 (2006).
15. A. Zanghellini *et al.*, *Protein Sci.* **15**, 2785 (2006).
16. Materials and methods are available as supporting material on *Science* Online.
17. J. Wagner, R. A. Lerner, C. F. Barbas III, *Science* **270**, 1797 (1995).
18. F. Tanaka, C. F. Barbas III, *J. Am. Chem. Soc.* **124**, 3510 (2002).
19. Single-letter abbreviations for the amino acid residues are as follows: A, Ala; C, Cys; D, Asp; E, Glu; F, Phe; G, Gly; H, His; I, Ile; K, Lys; L, Leu; M, Met; N, Asn; P, Pro; Q, Gln; R, Arg; S, Ser; T, Thr; V, Val; W, Trp; and Y, Tyr.
20. G. Dantas, B. Kuhlman, D. Callender, M. Wong, D. Baker, *J. Mol. Biol.* **332**, 449 (2003).
21. J. Meiler, D. Baker, *Proteins* **65**, 538 (2006).
22. W. H. Press, S. A. Teukolsky, W. T. Vetterling, B. P. Flannery, *Numerical Recipes in FORTRAN: The Art of Scientific Computing* (Cambridge Univ. Press, Cambridge, ed. 2, 1992).
23. F. R. Clemente, K. N. Houk, *J. Am. Chem. Soc.* **127**, 11294 (2005).
24. C. T. Porter, G. J. Bartlett, J. M. Thornton, *Nucleic Acids Res.* **32**, D129 (2004).
25. G. Zhong *et al.*, *Angew. Chem. Int. Ed. Engl.* **37**, 2481 (1998).

26. Kinetic parameters of the designs reported here were determined at the University of Washington. For selected designs, the kinetic parameters were confirmed by independent experiments performed at the Scripps Research Institute. We thank R. Fuller for technical assistance. Thorough testing of the four catalytic motifs was made possible through gene synthesis by Codon Devices. We thank Rosetta@Home participants for their valuable contributions of computer time. E.A.A. is funded by a Ruth L. Kirschstein National Research Service Award. This work was supported by the Defense Advanced Research Projects Agency and HHMI. Coordinates and structure factors for the crystal structures of RA22 variant S210A and RA61 variant M48K were deposited with the Research Collaboratory for Structural Bioinformatics Protein Data Bank (PDB) under the accession numbers 3B5V and 3B5L, respectively. The *xyz* coordinates of the designs RA22, RA34, RA45, RA46, RA60, and RA61 are included with the SOM as a zipped archive.

Supporting Online Material

www.sciencemag.org/cgi/content/full/319/5868/1387/DC1
Materials and Methods
SOM Text
Figs. S1 to S8
Tables S1 to S8
References
Design Model Coordinates in PDB Format

7 November 2007; accepted 5 February 2008
10.1126/science.1152692

A Cholesterol Biosynthesis Inhibitor Blocks *Staphylococcus aureus* Virulence

Chia-I Liu,[1,2,3]* George Y. Liu,[4]* Yongcheng Song,[5]* Fenglin Yin,[6] Mary E. Hensler,[7] Wen-Yih Jeng,[1,2] Victor Nizet,[7,8]† Andrew H.-J. Wang,[1,2,3]† Eric Oldfield[5,6]†

Staphylococcus aureus produces hospital- and community-acquired infections, with methicillin-resistant *S. aureus* posing a serious public health threat. The golden carotenoid pigment of *S. aureus*, staphyloxanthin, promotes resistance to reactive oxygen species and host neutrophil-based killing, and early enzymatic steps in staphyloxanthin production resemble those for cholesterol biosynthesis. We determined the crystal structures of *S. aureus* dehydrosqualene synthase (CrtM) at 1.58 angstrom resolution, finding structural similarity to human squalene synthase (SQS). We screened nine SQS inhibitors and determined the structures of three, bound to CrtM. One, previously tested for cholesterol-lowering activity in humans, blocked staphyloxanthin biosynthesis in vitro (median inhibitory concentration ~100 nM), resulting in colorless bacteria with increased susceptibility to killing by human blood and to innate immune clearance in a mouse infection model. This finding represents proof of principle for a virulence factor–based therapy against *S. aureus*.

Over the past 20 years, there has been an explosion in the prevalence of antibiotic-resistant bacterial infections, both in the hospital and in the general community; in the United States, more deaths are now attributable to methicillin-resistant *Staphylococcus aureus* (MRSA) infections than to HIV/AIDS (*1*, *2*). Unfortunately, over the same time, there has been a decrease in the rate of discovery of new antibiotics, creating a pressing need for the development of novel infectious disease therapies. One approach, discussed at a recent National Research Council workshop (*3*), involves the specific neutralization of bacterial virulence factors to render pathogenic bacteria susceptible to innate immune system clearance. However,

[1]Institute of Biological Chemistry, Academia Sinica, Nankang, Taipei 11529, Taiwan. [2]National Core Facility of High-Throughput Protein Crystallography, Academia Sinica, Nankang, Taipei 11529, Taiwan. [3]Institute of Biochemical Sciences, College of Life Science, National Taiwan University, Taipei 10098, Taiwan. [4]Division of Pediatric Infectious Diseases and Immunobiology Research Institute, Cedars-Sinai Medical Center, Los Angeles, CA 90048, USA. [5]Department of Chemistry, University of Illinois, Urbana, IL 61801, USA. [6]Center for Biophysics and Computational Biology, University of Illinois, Urbana, IL 61801, USA. [7]Department of Pediatrics, University of California, San Diego, La Jolla, CA 92093, USA. [8]Skaggs School of Pharmacy and Pharmaceutical Sciences, University of California, San Diego, La Jolla, CA 92093, USA.

*These authors contributed equally to this work.
†To whom correspondence should be addressed. E-mail: vnizet@ucsd.edu (V.N.); ahjwang@gate.sinica.edu.tw (A.H.-J.W.); eo@chad.scs.uiuc.edu (E.O.)

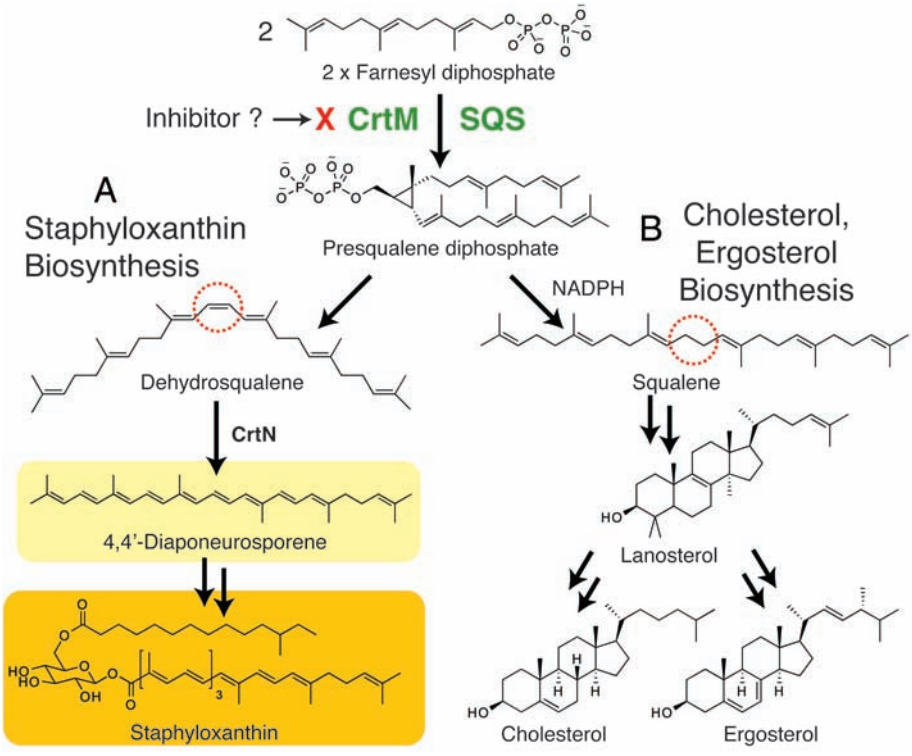

Fig. 1. Biosynthetic pathways. (**A**) Staphyloxanthin biosynthesis (in *S. aureus*). (**B**) Cholesterol (in humans) and ergosterol (in, e.g., yeasts and some parasitic protozoa) biosynthesis. Each biosynthetic pathway involves initial formation of presqualene diphosphate, catalyzed by CrtM (*S. aureus*) or by squalene synthase (SQS). In *S. aureus*, the NADPH reduction step is absent, resulting in production of dehydrosqualene, not squalene.

conventional screening campaigns are not well suited for selecting such inhibitors, because virulence factors typically do not affect bacterial cell growth but rather exert their activity in vivo. In *S. aureus*, an important virulence factor is the carotenoid pigment staphyloxanthin. This pigment acts as an antioxidant, with its numerous conjugated double bonds enabling the detoxification of host immune system–generated reactive oxygen species (ROS) such as O_2^-, H_2O_2, and HOCl (*4*, *5*). Bacteria that lack the carotenoid pigment grow normally, but they are rapidly killed by ROS from host neutrophils and are deficient in skin abscess formation (*4*). Blocking staphyloxanthin biosynthesis is therefore a potentially attractive therapeutic target (*3*, *4*), and the bright golden coloration of the virulence factor facilitates inhibitor screening.

The first committed step in staphyloxanthin biosynthesis, catalyzed by the *S. aureus* dehydrosqualene synthase (CrtM) enzyme, involves the 1,1′ or head-to-head condensation of two molecules of farnesyl diphosphate to produce the C_{30} species, presqualene diphosphate (*5*), which then undergoes skeletal rearrangement and further loss of diphosphate to produce dehydrosqualene (Fig. 1A). Successive dehydrogenations yield 4,4′-diaponeurosporene, which is then further oxidized, glycosylated, and esterified to give the carotenoid, staphyloxanthin (Fig. 1A). The structure of dehydrosqualene is very similar to that of the squalene used in cholesterol biosynthesis in humans, and both

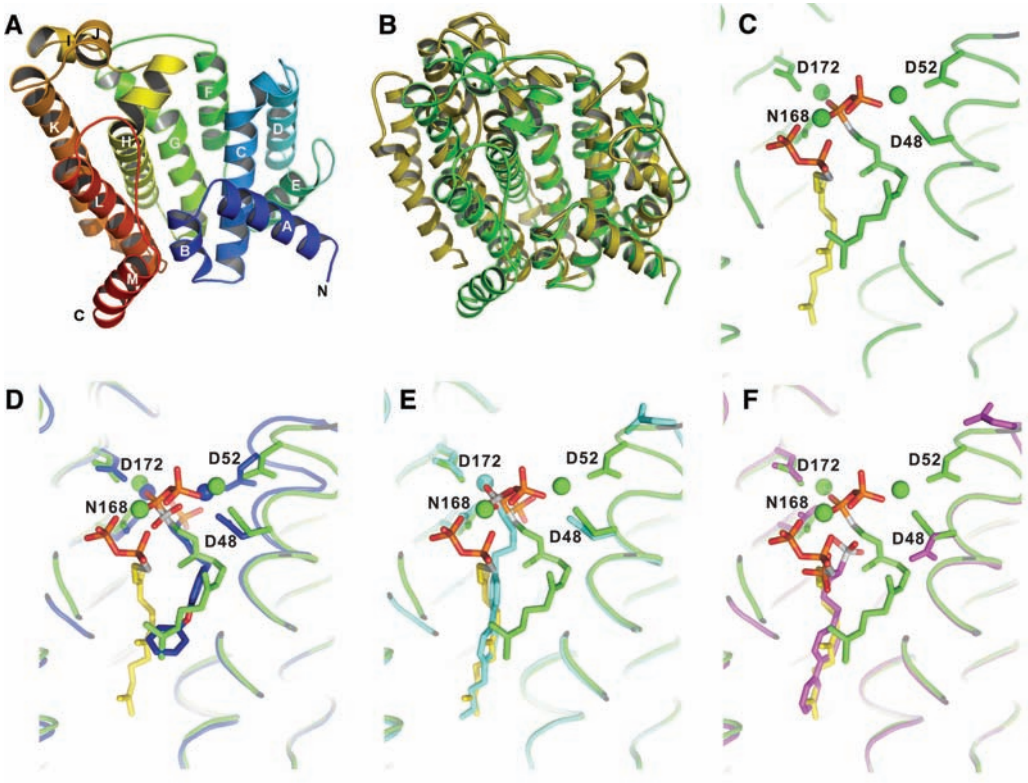

Fig. 2. X-ray crystallographic structures. (**A**) X-ray structure of *S. aureus* CrtM. (**B**) Superposition of CrtM and human squalene synthase structures. There is a 5.5 Å C_α RMS deviation between the two structures. (**C**) Close-up view of FsPP bound to CrtM. (**D**) Close-up view of *S. aureus* CrtM with bound BPH-652. (**E**) *S. aureus* CrtM with bound BPH-698. (**F**) *S. aureus* CrtM with bound BPH-700. In (C) to (F), the FsPP ligands are in green or yellow; BPH-652, BPH-698, and BPH-700 (and associated Mg^{2+}) are in blue, cyan, and magenta, respectively. Key contacts with Asp (D) and Asn (N) residues are indicated.

dehydrosqualene and squalene biosyntheses proceed through presqualene diphosphate. The pathways diverge at this intermediate, with a reduced nicotinamide adenine dinucleotide phosphate (NADPH)–catalyzed reductive step present in squalene synthesis but not in dehydrosqualene synthesis (Fig. 1B). Thus, *S. aureus* CrtM and human squalene synthase (SQS) might possess structural similarities, although only modest sequence homology (30% identity, 36% similarity) is found by Clustal (*6*) amino acid alignment (fig. S1). However, human SQS is known to have considerable structural similarity to other prenyl synthase enzymes, including farnesyl diphosphate synthase, pentalenene synthase, and 5-*epi*-aristolochene synthase, despite the lack of sequence homology (*7*).

To probe this structural question, we cloned, expressed, purified, and crystallized the CrtM protein from *S. aureus* and solved its structure by x-ray crystallography to 1.58 Å. Data collection and refinement statistics for the selenomethionine-substituted and wild-type proteins are presented in tables S1 and S2. CrtM crystallizes in the $P3_221$ space group and there is one molecule per asymmetric unit. The overall fold (Fig. 2A) shows clear similarity to that seen in human SQS (PDB accession number 1EZF), as can be seen in the superposition (Fig. 2B), with a 5.5 Å root-mean-square (RMS) deviation between the C_α atoms in the two structures. CrtM is all helical and has a large central cavity (also seen in other isoprenoid synthases) capable of accommodating the C_{30} product, dehydrosqualene.

To see how inhibitors might bind to CrtM, we first crystallized the protein with farnesyl thiodiphosphate (FsPP, Fig. 3), a nonreactive analog of farnesyl diphosphate, the substrate for CrtM. FsPP has previously been found to be a substrate-analog inhibitor of other prenyl transferases, including geranylgeranyl diphosphate synthase and undecaprenyl diphosphate synthase (*8*). However, in each of those structures, only one FsPP binds per protein. In CrtM, however, two FPP molecules must come together to form dehydrosqualene, and indeed, two FsPP molecules were found in the large central cavity (Fig. 2C). Their diphosphate head groups interact with three Mg^{2+} ions, which in turn interact with Asp residues in the two conserved Asp-X-X-X-Asp repeats (fig. S1) seen in many prenyl synthases. The space group of FsPP•CrtM is $P3_121$, and there are two molecules per asymmetric unit. Electron densities for the two ligands and key protein-ligand interactions are shown in figs. S2 and S3. This ligand binding pattern is likely to define the location of the presqualene diphosphate intermediate binding site.

Structural similarity raised the possibility that human SQS inhibitors developed as potential cholesterol-lowering drugs (*9*–*12*) might also be active against CrtM. We synthesized eight such compounds (Fig. 3) and tested them for activity in CrtM inhibition (*13*). There is considerable structural diversity among these compounds: Some mimic the FPP substrate (e.g., the phosphonosulfonates BPH-652, BPH-698, and BPH-700); others presumably act as analogs of carbocations or transition states (e.g., the amines, BPH-651, BPH-661, and BPH-673); and others, such as the dicarboxylic acid BPH-660, have a less certain mechanism of action.

Of the eight compounds tested, only the three phosphonosulfonates were found to be CrtM inhibitors (BPH-652, inhibitor constant K_i = 1.5 nM; BPH-698, K_i = 135 nM; BPH-700, K_i = 6 nM; fig. S4). Each phosphonosulfonate also had potent activity against *S. aureus* pigment formation in vitro, as shown for BPH-652 in Fig. 4A, with median inhibitory concentration (IC_{50}) values in the range 100 to 300 nM (Fig. 4B). The bisphosphonate BPH-674 (Fig. 3) was a more potent CrtM inhibitor (K_i = 0.2 nM; fig. S4) than any of the phosphonosulfonates

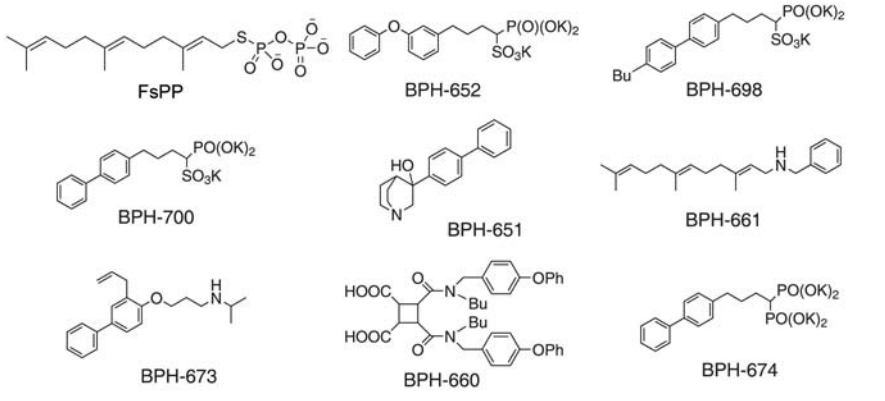

Fig. 3. Chemical structures of farnesyl thiodiphosphate (FsPP) and eight squalene synthase inhibitors. There are many different types of SQS inhibitor, but only the phosphonosulfonates (and related bisphosphonates) inhibit CrtM. To date, only the phosphonosulfonates have been found to have activity in *S. aureus*.

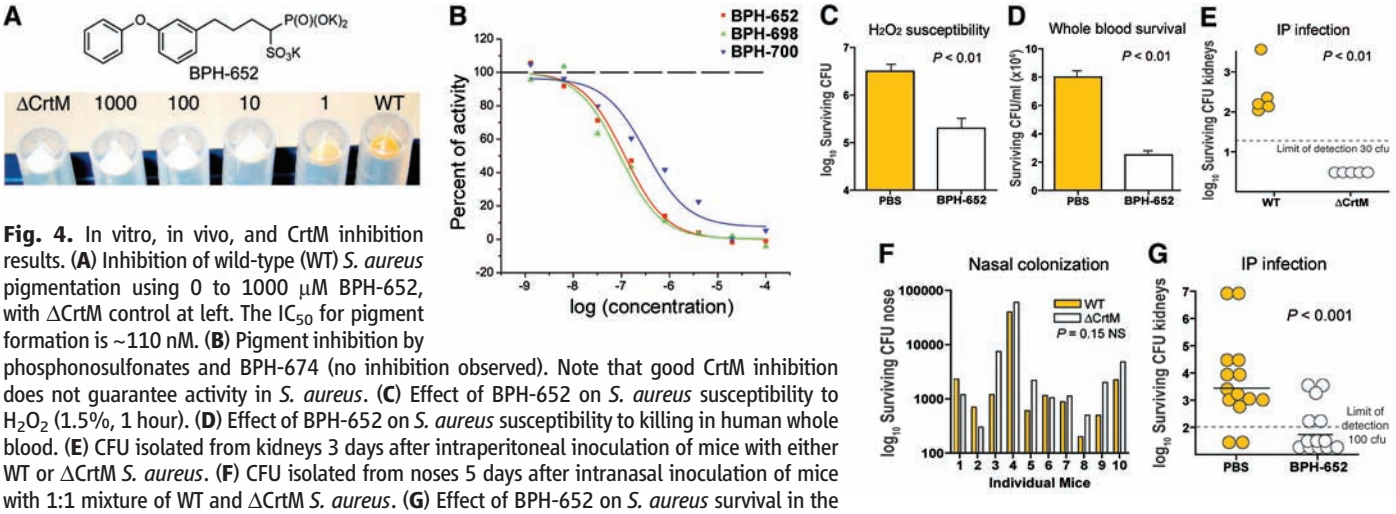

Fig. 4. In vitro, in vivo, and CrtM inhibition results. (**A**) Inhibition of wild-type (WT) *S. aureus* pigmentation using 0 to 1000 μM BPH-652, with ΔCrtM control at left. The IC_{50} for pigment formation is ~110 nM. (**B**) Pigment inhibition by phosphonosulfonates and BPH-674 (no inhibition observed). Note that good CrtM inhibition does not guarantee activity in *S. aureus*. (**C**) Effect of BPH-652 on *S. aureus* susceptibility to H_2O_2 (1.5%, 1 hour). (**D**) Effect of BPH-652 on *S. aureus* susceptibility to killing in human whole blood. (**E**) CFU isolated from kidneys 3 days after intraperitoneal inoculation of mice with either WT or ΔCrtM *S. aureus*. (**F**) CFU isolated from noses 5 days after intranasal inoculation of mice with 1:1 mixture of WT and ΔCrtM *S. aureus*. (**G**) Effect of BPH-652 on *S. aureus* survival in the kidney after intraperitoneal infection. In vitro data shown are representative of at least three identical experiments. In vivo data in (G) are compiled from two sets of experiments, using different numbers of mice, performed under the same conditions (*13*).

but had no activity at all in pigment inhibition in vitro, due perhaps to poor bacterial cell uptake or increased efflux. None of the four amine/carboxylate human SQS inhibitors had any activity in inhibiting CrtM or pigment formation, although all are known to be potent human SQS inhibitors. Taken together, these results pointed to phosphonosulfonates as being the most promising class of CrtM inhibitors for further investigation, beginning with structure determination.

All three phosphonosulfonates, BPH-652, BPH-698, and BPH-700, yielded well-resolved $2F_{obs} - F_{calc}$ densities (fig. S5); the refined structures obtained are shown in Fig. 2, D to F, superimposed on the FsPP structure. Full crystallographic details are given in table S2, and ligand interaction results are shown in figs. S6 to S8. Interestingly, in all three structures, we found evidence for only one phosphonosulfonate bound per CrtM, not the two ligands that might have been anticipated from the FsPP structure. Moreover, all three inhibitors have different binding modes. BPH-652 (Fig. 2D) binds into the FsPP-1 site with two Mg^{2+}, BPH-698 binds into the FsPP-2 site (Fig. 2E) with only one Mg^{2+}, and BPH-700 binds into the FsPP-2 site with no Mg^{2+} (Fig. 2F). The phosphonosulfonate side chains do, however, closely track the locations of the two FsPP inhibitor side chains. FsPP-1 is highly bent (green structure in Fig. 2C), and BPH-652 is able to track this bent geometry (Fig. 2D), due at least in part to the presence of its central ether O atom. On the other hand, the (linear) biphenyl side chains in the BPH-698 and BPH-700 structures can be closely superimposed on the fully extended farnesyl side chain in the FsPP-2 site (yellow in Fig. 2, C, E, and F). Additional views of all superimposed ligands are shown in fig. S9.

Although the aryl side chains in the two biphenyl phosphonosulfonates are closely aligned (Fig. 2, E and F), the head groups bind very differently. With BPH-698, the phosphonosulfonate head group is involved in electrostatic interactions with one Mg^{2+}, but in BPH-700 (which lacks the 4′-butyl side chain), no Mg^{2+} is found in the structure; instead, the phosphonosulfonate is involved in electrostatic or hydrogen bond interactions with His^{18} and Tyr^{41}. With all three phosphonosulfonate inhibitors, electrostatic interactions between ligand and protein are important, with eight or nine highly hydrophobic amino acid side chains contacting the inhibitor side chains.

To probe the possible use of a phosphonosulfonate CrtM inhibitor as an antimicrobial, we performed a series of experiments to determine whether such a compound was (i) nontoxic to mammalian cells, (ii) able to restore *S. aureus* killing by oxidants and phagocytes, and (iii) able to limit *S. aureus* disease progression in vivo. BPH-652 was selected for these experiments because it has a good IC_{50} in pigment inhibition (110 nM; Fig. 4B) and because *S*-BPH-652 (and its analogs) have been advanced through preclinical testing in rats and in two human clinical trials (*14*, *15*) as cholesterol-lowering agents.

As expected, BPH-652 had no effect on the growth of three human cell lines (MCF-7, NCI-H460, and SF-268), because only cholesterol biosynthesis is targeted and cholesterol is generally abundant in serum (or diet). This indicates low toxicity, consistent with the results of the clinical trials (on *S*-BPH-652). Also, incubation with up to 2 mM BPH-652 affected neither *S. aureus* growth characteristics nor survival through 48 hours in culture. However, after incubation with 100 μM BPH-652, the resulting nonpigmented (white) *S. aureus* were more susceptible to killing by 1.5% hydrogen peroxide by a factor of ~15, and, relative to normally pigmented *S. aureus* treated with phosphate-buffered saline (PBS) control, were less able to survive in freshly isolated human whole blood by a factor of ~4 (Fig. 4, C and D), as expected because they contained no carotenoid pigment to act as an antioxidant.

Finally, we sought to establish whether inhibition of staphyloxanthin biosynthesis by BPH-652 could represent a purely virulence factor–based therapy against *S. aureus* infection. We first extended our previous observations on the contribution of staphyloxanthin to abscess formation (*4*) to a systemic *S. aureus* infection model. Staphyloxanthin was found to promote invasive disease potential, because mice inoculated with 10^8 colony-forming units (CFU) of wild-type *S. aureus* (by intraperitoneal injection) developed a sustained infection, with bacteria recovered from the kidneys 72 hours later; an isogenic *S. aureus* mutant lacking the CrtM enzyme was cleared by the host after similar challenge (Fig. 4E). Conversely, the contribution of *S. aureus* pigmentation to mucosal colonization after intranasal inoculation was negligible (Fig. 4F). These data are consistent with a primary function of staphyloxanthin in resisting the host oxidant-based phagocytic defenses that are present in disease contexts but are absent on mucosal surfaces without inflammation.

Under the same intraperitoneal challenge used in Fig. 4E, we then treated one group of mice ($n = 14$) with 0.5 mg of BPH-652 twice per day (days –1, 0, 1, and 2), and a second group ($n = 13$) with equivalent volume injections of PBS control. Upon killing at 72 hours, *S. aureus* bacterial counts in the kidneys of the mice treated with BPH-652 were significantly lower than those of the control group ($P < 0.001$), with 8 of 13 below the detection threshold, versus only 2 of 14 in the control group (Fig. 4G); on average, this result corresponds to a 98% decrease in surviving bacteria in the treatment group.

Thus, the CrtM (dehydrosqualene synthase) enzyme from *S. aureus* is a target for anti-infective therapy based on virulence factor neutralization, and a drug candidate already tested in humans in the context of cholesterol-lowering therapy provides a good lead. These results therefore provide a basis for rational drug design against this major human pathogen, and provide proof of principle of the utility of an anti-infective drug without direct bactericidal properties that instead renders the pathogen susceptible to normal host innate immune clearance. Our approach, and other virulence factor–based concepts (*16*, *17*) for highly specific antistaphylococcal therapy, also offer theoretical advantages for reducing selection pressure toward the emergence of resistance, both in the pathogen and in our normal commensal microflora (*3*, *18*).

References and Notes

1. E. A. Bancroft, *JAMA* **298**, 1803 (2007).
2. R. M. Klevens *et al.*, *JAMA* **298**, 1763 (2007).
3. National Research Council, in *Treating Infectious Diseases in a Microbial World: Report of Two Workshops on Novel Antimicrobial Therapeutics* (National Academies Press, Washington, DC, 2006), pp. 21–22.
4. G. Y. Liu *et al.*, *J. Exp. Med.* **202**, 209 (2005).
5. A. Clauditz, A. Resch, K. P. Wieland, A. Peschel, F. Gotz, *Infect. Immun.* **74**, 4950 (2006).
6. J. D. Thompson, D. G. Higgins, T. J. Gibson, *Nucleic Acids Res.* **22**, 4673 (1994).
7. J. Pandit *et al.*, *J. Biol. Chem.* **275**, 30610 (2000).
8. R. T. Guo *et al.*, *Proc. Natl. Acad. Sci. U.S.A.* **104**, 10022 (2007).
9. H. Hiyoshi *et al.*, *J. Lipid Res.* **41**, 1136 (2000).
10. T. Nishimoto *et al.*, *Br. J. Pharmacol.* **139**, 911 (2003).
11. T. Ishihara *et al.*, *Bioorg. Med. Chem.* **11**, 2403 (2003).
12. D. R. Magnin *et al.*, *J. Med. Chem.* **39**, 657 (1996).
13. See supporting material on *Science* Online.
14. A. Sharma, P. H. Slugg, J. L. Hammett, W. J. Jusko, *Pharm. Res.* **15**, 1782 (1998).
15. A. Sharma, P. H. Slugg, J. L. Hammett, W. J. Jusko, *J. Clin. Pharmacol.* **38**, 1116 (1998).
16. H. Ton-That, O. Schneewind, *J. Biol. Chem.* **274**, 24316 (1999).
17. G. J. Lyon, P. Mayville, T. W. Muir, R. P. Novick, *Proc. Natl. Acad. Sci. U.S.A.* **97**, 13330 (2000).
18. L. E. Alksne, S. J. Projan, *Curr. Opin. Biotechnol.* **11**, 625 (2000).

19. Supported by U.S. Public Health Service grants AI07482 (G.Y.L.), HD051796 (V.N.), and GM073216 and GM65307 (E.O.); Academia Sinica and National Core Facility of High-Throughput Protein Crystallography grant NSC95-3112-B-001-015-Y (A.H.-J.W.); a Burroughs-Wellcome Career Award (G.Y.L.); and a Leukemia and Lymphoma Society Special Fellowship (Y.S.). We thank K. Krysiak for carrying out the mammalian cell growth inhibition assays. Diffraction data were obtained at the National Synchrotron Radiation Research Center of Taiwan, SPring-8 and the Photon Factory in Japan, and at the Advanced Light Source, Berkeley, CA. The coordinates for the CrtM, FsPP, BPH-652, BPH-698, and BPH-700 structures have been deposited in the Protein Data Bank under accession numbers 2ZCO, 2ZCP, 2ZCQ, 2ZCR, and 2ZCS, respectively.

Supporting Online Material

www.sciencemag.org/cgi/content/full/1153018/DC1
Materials and Methods
Figs. S1 to S9
Tables S1 and S2
References

15 November 2007; accepted 28 January 2008
Published online 14 February 2008;
10.1126/science.1153018
Include this information when citing this paper.